Available online at www.sciencedirect.com
ScienceDirect
Journal of Solid State Chemistry 180 (2007) 3333–3340
JOURNAL OF SOLID STATE CHEMISTRY
www.elsevier.com/locate/jssc

Formation, structure and magnetism of the metastable defect fluorite phases $AVO_{3.5+x}$ (A = In, Sc)

Shahid P. Shafi[a], Rylan J. Lundgren[a], Lachlan M.D. Cranswick[b], Mario Bieringer[a,*]

[a]*Department of Chemistry, University of Manitoba, Winnipeg, MB, Canada R3T 2N2*
[b]*Canadian Neutron Beam Centre, National Research Council Canada, Chalk River Laboratories, Chalk River, ON, Canada K0J 1J0*

Received 10 July 2007; received in revised form 21 September 2007; accepted 21 September 2007
Available online 1 October 2007

Abstract

We report the preparation and stability of $ScVO_{3.5+x}$ and the novel phase $InVO_{3.5+x}$. $AVO_{3.5+x}$ (A = Sc, In) defect fluorite structures are formed as metastable intermediates during the topotactic oxidation of AVO_3 bixbyites. The oxidation pathway has been studied in detail by means of thermogravimetric/differential thermal analysis and in-situ powder X-ray diffraction. The oxidation of the bixbyite phase follows a topotactic pathway at temperatures between 300 and 400 °C in air/carbon dioxide. The range of accessible oxygen stoichiometries for the $AVO_{3.5+x}$ structures following this pathway are $0.00 \leqslant x \leqslant 0.22$. Rietveld refinements against powder X-ray and neutron data revealed that $InVO_{3.54}$ and $ScVO_{3.70}$ crystallize in the defect fluorite structure in space group $Fm\text{-}3m$ (227) with $a = 4.9863(5)$ and 4.9697(3)Å, respectively with A^{3+}/V^{4+} disorder on the (4*a*) cation site. Powder neutron diffraction experiments indicate clustering of oxide defects in all samples. Bulk magnetic measurements showed the presence of V^{4+} and the absence of magnetic ordering at low temperatures. Powder neutron diffraction experiments confirmed the absence of a long range ordered magnetic ground state.
© 2007 Elsevier Inc. All rights reserved.

Keywords: Defect fluorite structure; Bixbyite structure; Topotactic oxidation; In-situ X-ray diffraction; Thermal analysis; Powder neutron diffraction; InVO_(3.5+x); ScVO_(3.5+x); Low temperature magnetism

1. Introduction

Rare-earth orthovanadates, AVO_3 (A = La–Lu) show very diverse crystallographic varieties and physical properties such as low temperature magnetic transitions coupled to crystallographic transitions, canted antiferromagnetic ground states with orbital ordering [1,2] and magnetic field dependent as well as temperature induced spin reversal [3–5]. These properties are closely related to the perovskite structure and its inherent ability to tolerate octahedral distortions, orbital ordering, cation substitution and to undergo cooperative octahedral tilting in order to accommodate various trivalent A-cation sizes. For the perovskite structure the mismatch between the A^{3+} cation and the octahedral vanadium oxide network increases towards the heavier rare-earth cations. A^{3+} cations smaller than Lu^{3+} such as In^{3+} [6] and Sc^{3+} [7,8] form AVO_3 bixbyite phases with A^{3+}/V^{3+} disorder on the octahedral cation sites. Notably, the solid solution $Sc_{(1-x)}Lu_xVO_3$ crystallizes in the perovskite structure for $x > 0.58$, whereas the Sc rich regime forms bixbyite structures at high temperature only for $x < 0.1$ [9]. However $Sc_{(1-x)}Lu_xVO_3$ bixbyite phases with $0.1 < x < 0.4$ can be prepared as metastable products at fairly low temperatures (600 °C) [9]. In 2004, Alonso et al. [8] reported the formation of the defect fluorite structure, $ScVO_{3.5}$, with 1/8 statistically distributed oxygen vacancies during the topotactic oxidation of $ScVO_3$ at 350 °C. During the second oxidation step $ScVO_{3.5}$ oxidizes to the zircon structure, $ScVO_4$, with V^{5+}-O_4 tetrahedral units [10]. The oxidation processes involved during the two-step reaction have never been investigated structurally. Only two AVO_3 bixbyite phases hypothetically capable of undergoing two-step oxidations are known, namely $ScVO_3$ and $InVO_3$. The indium vanadium oxide and scandium vanadium oxide phase diagrams only consist of a very limited number of

*Corresponding author. Fax: +204 474 7608.
E-mail address: Mario_Bieringer@umanitoba.ca (M. Bieringer).

0022-4596/$ - see front matter © 2007 Elsevier Inc. All rights reserved.
doi:10.1016/j.jssc.2007.09.028

compounds, namely, AVO_3 [6–9], AVO_4 [10–12], In_2VO_5 [13] and $ScVO_{3.5}$ [8]. To date no indium or scandium vanadium oxide pyrochlore structures have been reported. We report the preparation of the new defect fluorite phases $InVO_{3.5+x}$ and furthermore investigate the ranges of oxygen stoichiometries, x, for $ScVO_{3.5+x}$ and $InVO_{3.5+x}$. For the first time the reaction pathways of the topotactic oxidation of bixbyite orthovanadates to the defect fluorite structure and the final oxidation to the zircon structure are followed by in-situ X-ray diffraction and thermogravimetric analysis (TGA). The bulk preparation and magnetic properties of $AVO_{3.5+x}$ (A = Sc, In) are reported. Notably defect oxide structures are particularly interesting as potential ion conductors, in fact the defect fluorite structure and the pyrochlore structure are both part of the four structural groups of important oxide ion conductors [14,15]. $ScVO_{3.5+x}$ and $InVO_{3.5+x}$ are potential candidates for ion conductor applications.

2. Experimental

2.1. Synthesis

Polycrystalline $AVO_{3.5}$ bulk samples were prepared by a three-step synthesis via AVO_4 and AVO_3. All samples were ground in an agate mortar under acetone and reacted in alumina crucibles. The AVO_4 precursors were obtained by solid-state reaction of In_2O_3 (Alfa Aesar, 99.995%) or Sc_2O_3 (Alfa Aesar 99.995%) and NH_4VO_3 (CERAC, 99.9%)[1] at 1000 °C for 20 h in air according to

$$A_2O_3 + 2NH_4VO_3 \rightarrow 2AVO_4 + 2NH_3 + H_2O. \quad (1)$$

The cream coloured $InVO_4$ sample contained small amounts (1%) of In_2O_3 impurity, the pale yellow $ScVO_4$ was phase pure. The reduction of $InVO_4$ in CO/CO_2 (1:1) flow at 450 °C for 12 h according to [6] resulted in black polycrystalline $InVO_3$ with 1.5% In_2O_3 impurity. $ScVO_4$ was reduced under the same conditions at 1000 °C and resulted in dark brown phase pure $ScVO_3$.

$$AVO_4 + CO \rightarrow AVO_3 + CO_2. \quad (2)$$

Bulk samples of black polycrystalline $InVO_{3.5}$ were prepared by mild oxidation of a thin layer (cast from an acetone slurry) of $InVO_3$ in CO_2 at 350 °C for 44 h according to Eq. (3). Black $ScVO_{3.5}$ was prepared at 350 °C in air according to Eq. (4).

$$2InVO_3 + CO_2 \rightarrow 2InVO_{3.5} + CO, \quad (3)$$

$$2ScVO_3 + \tfrac{1}{2}O_2 \rightarrow 2ScVO_{3.5}. \quad (4)$$

Bulk $InVO_{3.5}$ contained 2% In_2O_3 impurity and $ScVO_{3.5}$ was phase pure. In addition the low temperature bixbyite phase $Sc_{0.8}Lu_{0.2}VO_3$ was prepared according to Ref. [9] at 600 °C.

[1]Small amounts of vanadium oxide loss were compensated for with 2 mol% excess NH_4VO_3.

2.2. Powder X-ray diffraction

Polycrystalline products were identified by powder X-ray diffraction using a PANalytical X'Pert Pro diffractometer in Bragg–Brentano configuration using $K\alpha_{1,2}$(λ = 1.540598, 1.544426 Å) radiation equipped with a diffracted beam Ni-filter and an X'Celerator detector. Room temperature diffractograms were collected over the 2θ-range 10–90° with 0.0167° steps. All reported unit cell dimensions and initial structural refinements were carried out with the Rietveld package FullProf 2003 [16].

2.3. In-situ powder X-ray diffraction

In-situ powder X-ray diffraction experiments were carried out on a PANalytical X'Pert Pro diffractometer equipped with an X'Celerator detector and an Anton Paar HTK2000 high temperature camera. The samples were heated on a resistive platinum strip heater. The diffraction experiments were performed with Cu$K\alpha_{1,2}$(λ = 1.540598, 1.544426 Å) radiation for the angular range 2θ = 15–70° with 0.0167° step size. The AVO_3 samples were mounted as thin layers on a platinum heating element and heated from 25 to 800 °C. $InVO_3$ was oxidized in CO_2 using 25 °C increments whereas $ScVO_3$ was oxidized in air using 10 °C increments.

2.4. Powder neutron diffraction

Powder neutron diffraction data were collected on the medium-resolution 800 wire diffractometer C2 operated by the National Research Council Canada at Chalk River. The diffraction patterns at room temperature and at 3 K were measured with neutron wavelengths λ = 2.37192 and 1.33052 Å and default wire spacing of 0.1002°. The Rietveld analyses of all bulk samples were carried out as simultaneous powder neutron and powder X-ray refinements using FullProf 2003 [16].

2.5. Thermogravimetric analysis/differential thermal analysis (TGA/DTA)

Simultaneous TGA/DTA experiments were carried out with a Linseis L81 thermobalance. All $AVO_{3.5+x}$ phases were fully oxidized in oxygen flow with a heating rate of 10 °C/min from 25 to 1000 °C. All experiments were corrected for buoyancy and were conducted in alumina crucibles with Al_2O_3 powder as the reference. The products were identified by powder X-ray diffraction.

2.6. Magnetic property measurements

Bulk d.c. magnetic susceptibility measurements were carried out with a Quantum Design MPMS SQUID magnetometer in an applied field of 0.1 T for the temperature range 5–325 K. The sample was placed in a gelatin capsule and held in a plastic straw. Zero-field

cooled data were measured during heating after having cooled the sample in the absence of an external magnetic field; the field-cooled data were measured after cooling in an external magnetic field of 0.1 T.

3. Results and discussion

3.1. In-situ powder X-ray diffraction

The oxidation pathways of AVO_3 bixbyite phases were followed by in-situ powder X-ray diffraction in 10 °C and 25 °C increments from 25 to 800 °C for $ScVO_3$ and $InVO_3$ respectively. Fig. 1a and b show the contour plots of the temperature dependent powder X-ray diffraction data during oxidation of $ScVO_3$ in air and $InVO_3$ in CO_2, respectively. Upon heating the $ScVO_3$ (222) and (400) peaks persist until approximately 325 °C. New diffraction peaks indicate an intermediate phase between 300 and 525 °C. The diffraction patterns can be indexed on a cubic unit cell consistent with space group *Fm*-3*m* and are in agreement with the recently reported oxygen defect fluorite structure $ScVO_{3.5}$ [8]. Notably, the new peaks show large, continuous shifts towards lower diffraction angles in this temperature range indicating a large range of oxygen uptake during oxidation, thus the structure is better described as $ScVO_{3.5+x}$. The metastable defect fluorite structure can only be prepared in a limited temperature range. Oxidation to the final product $ScVO_4$ occurs at 500 °C. Fig. 1b shows the oxidation of $InVO_3$ in CO_2 flow. The similarities of the contour maps indicate that both bixbyite phases undergo oxidation to AVO_4 via the analogous intermediates $AVO_{3.5+x}$. $InVO_{3.5}$ formation sets in at 250 °C and the phase persists until 450 °C, with the subsequent formation of $InVO_4$ just below 425 °C. Similar to $ScVO_{3.5+x}$ the indium analogue can accommodate a range of oxygen stoichiometries. The in-situ oxidation of the bixbyite phase $Sc_{0.8}Lu_{0.2}VO_3$ also showed the formation of the $Sc_{0.8}Lu_{0.2}VO_{3.5+x}$ defect fluorite structure intermediate at low temperature, thus supporting a topotactic reaction pathway. In contrast Lu-rich perovskite members oxidize in a single step to the corresponding zircon structures. This supports that only the bixbyite structure can undergo topotactic oxidation for the AVO_3 system. $ScVO_{3.5+x}$ and $InVO_{3.5+x}$ can exist as single phases only in limited temperature ranges under the above mentioned oxidation conditions. Oxidation of $InVO_3$ in air does not permit the preparation of a pure $InVO_{3.5+x}$ phase, instead $InVO_4$ is formed before $InVO_3$ is entirely consumed. Fig. 2 shows the Rietveld plot of the defect fluorite structure $InVO_{3.5+x}$ against powder X-ray diffraction data measured at 350 °C during the in-situ oxidation of $InVO_3$. Fig. 3a shows the unit cell evolution of $InVO_3$ and $InVO_{3.5+x}$ during in-situ oxidation obtained from Rietveld refinements. The sudden increase of the cubic unit cell axis for $InVO_3$ at 150 °C suggests the onset of oxygen uptake into the bixbyite structure. The defect fluorite $InVO_{3.5+x}$ is first observed at 225 °C with a considerable increase of the cubic unit cell axis up to 400 °C. The thermal expansion of $InVO_{3.54}$ was determined in a separate in-situ diffraction experiment in dynamic vacuum. In Fig. 3a the slope of the unit cell parameter evolution due to thermal expansion is compared with the unit cell

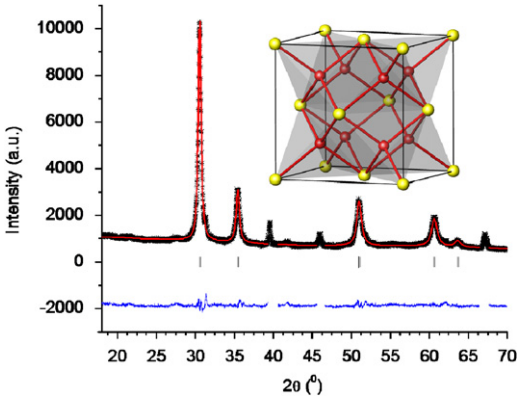

Fig. 2. $InVO_{3.5+x}$ (space group: *Fm*-3*m*) Rietveld plot of powder X-ray pattern measured at 350 °C during the in-situ oxidation of $InVO_3$. Three platinum peaks originating from the heater have been excluded from the refinement. The weak high-angle shoulders on the intense peaks correspond to traces of the starting material $InVO_3$. The fluorite structure with cation positions in red and anion positions in yellow is illustrated in the inset.

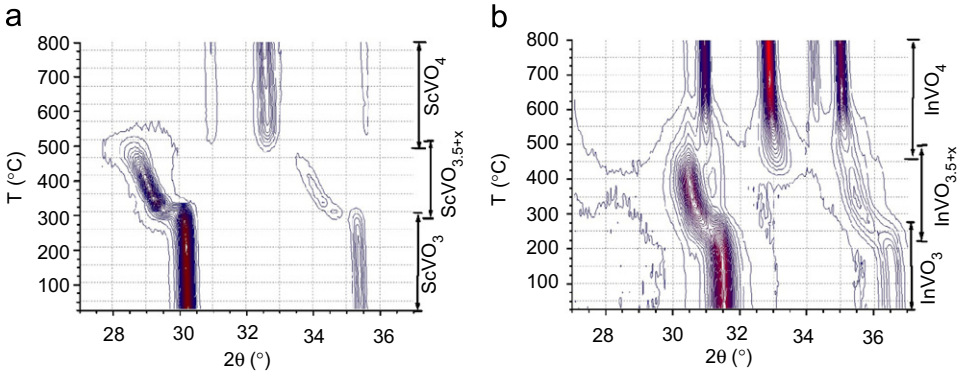

Fig. 1. (a) Powder X-ray diffraction contour plot of $ScVO_3$ oxidation in air from 25 to 800 °C with 10 °C increments. (b) Powder X-ray diffraction contour plot of $InVO_3$ oxidation in CO_2 flow from 25 to 800 °C with 25 °C increments. Intensities are shown as constant increments from blue = lowest intensity to red = highest intensity.

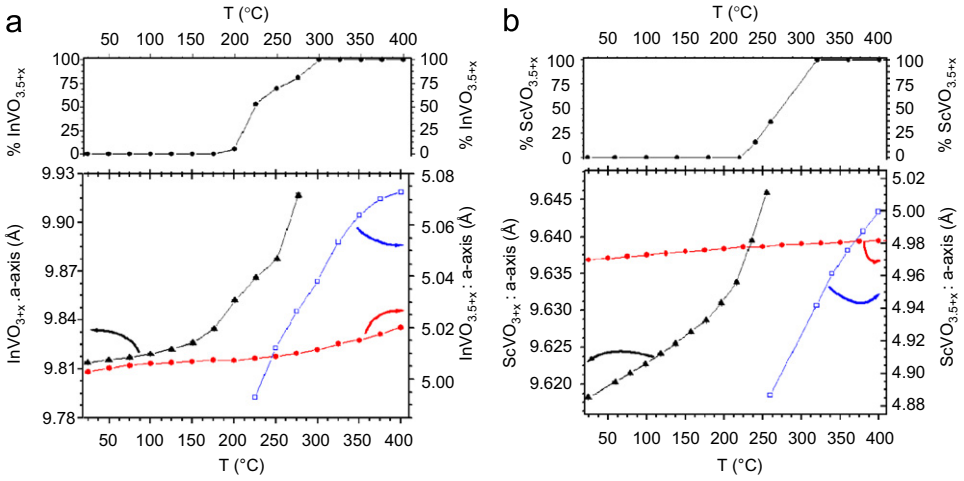

Fig. 3. (a) Unit cell parameter evolution of $InVO_3$ (solid triangles) and $InVO_{3.5+x}$ (open blue squares) during in-situ oxidation as obtained from Rietveld refinements. The unit cell evolution of $InVO_{3.54}$ in vacuum (solid red circles) shows the thermal expansion of $InVO_{3.54}$. The phase fraction of $InVO_{3.5+x}$ is indicated in the upper panel. (b) Unit cell parameter evolution of $ScVO_3$ (solid triangles) and $ScVO_{3.5+x}$ (open blue squares) during in-situ oxidation as obtained from Rietveld refinements. The unit cell evolution of $ScVO_{3.70}$ in vacuum (solid red circles) shows the thermal expansion of $ScVO_{3.70}$. The phase fraction of $ScVO_{3.5+x}$ is indicated in the upper panel.

expansion during oxidation of $InVO_3$. All unit cell parameters were determined by means of Rietveld refinement. The increased slope of the $InVO_{3.5+x}$ unit cell parameter beyond 250 °C suggests additional oxygen uptake during heating in CO_2. The upper panel of Fig. 3a shows the $InVO_{3.5+x}$ phase fraction as obtained from Rietveld refinements. Fig. 3b shows the unit cell parameter evolution of $ScVO_3$ and $ScVO_{3.5+x}$ in oxygen flow and the thermal expansion of $ScVO_{3.70}$ in vacuum. Note the coinciding unit cell parameters at approximately 370 °C close to the maximum cell parameter as determined during the in-situ oxidation. The phase fraction of $ScVO_{3.5+x}$ during oxidation is shown in the upper panel of Fig. 3b.

3.2. Bulk oxidation of $InVO_3$ and thermogravimetric oxidation of $InVO_{3.5+x}$

$InVO_{3.5+x}$ bulk samples were synthesized through $InVO_3$ oxidation in CO_2. Controlled oxidation only succeeded for thin layers, whereas $InVO_3$ pellets did not show any appreciable oxidation. Fig. 4 compares the powder X-ray diffractograms of $InVO_3$ and the oxidation products of a pelletized and thin layer sample. Oxidation in air or oxygen resulted in $InVO_4$ contaminated samples. A series of $InVO_{3.5+x}$ bulk samples was prepared and oxygen stoichiometries were determined thermogravimetrically in oxygen flow according to

$$2InVO_{3.5+x} + (1/2 - x)O_2 \rightarrow 2InVO_4. \quad (5)$$

The oxygen concentrations for the defect fluorite structure $InVO_{3.5+x}$ range from $InVO_{3.50(2)}$ to $InVO_{3.72(2)}$. The cubic unit cell parameter as determined by Rietveld refinements against powder X-ray diffraction data increases monotonically with increasing oxygen content in $InVO_{3.5+x}$. The thermogravimetric analyses proved that the oxygen content

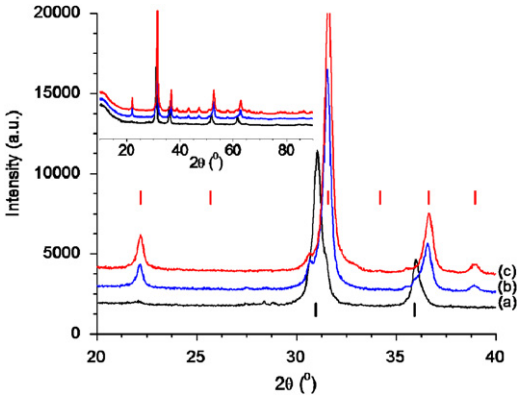

Fig. 4. Powder X-ray diffractograms of (a) $InVO_3$ oxidized as a flat layer, (b) $InVO_3$ oxidized as a pellet and (c) pristine $InVO_3$. The upper and lower tick marks correspond to $InVO_3$ and $InVO_{3.5}$ Bragg positions, respectively. $InVO_{3.5}$ is only formed if $InVO_3$ is oxidized as a thin layer.

Table 1
Correlation of cubic unit cell axis parameter with oxygen content in $InVO_{3.5+x}$ determined thermogravimetrically by oxidation to $InVO_4$

Oxygen content	*a*-axis (Å)
$InVO_{3.50(1)}$	4.9785(3)
$InVO_{3.53(1)}$	4.9822(2)
$InVO_{3.54(1)}$	4.9873(2)
$InVO_{3.65(1)}$	5.0037(3)
$InVO_{3.72(1)}$	5.0075(2)

varied in each of the products formed. The results are shown in Table 1. Though the oxidation of $InVO_{3.5}$ in CO_2 during the in-situ powder X-ray diffraction experiment was successful the thermogravimetric results during oxidation of a thin layer were not conclusive due to the small sample mass. Simultaneous thermogravimetric and DTA of $InVO_3$

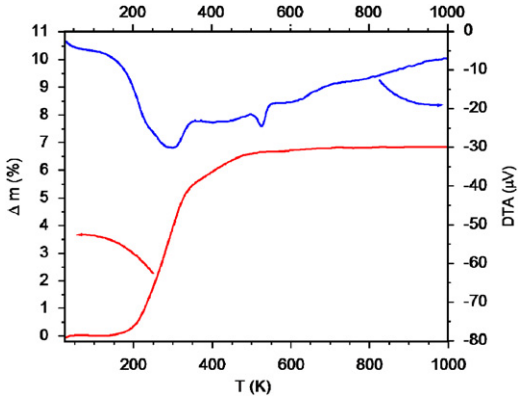

Fig. 5. Thermogravimetric (TGA) and differential thermal analysis (DTA) of $InVO_3$ oxidation in oxygen flow using a heating rate of 10 °C/min. The two major peaks for the DTA reveal two oxidation steps. The mass gain for the thermogravimetric data shows severe overlap of both oxidation steps.

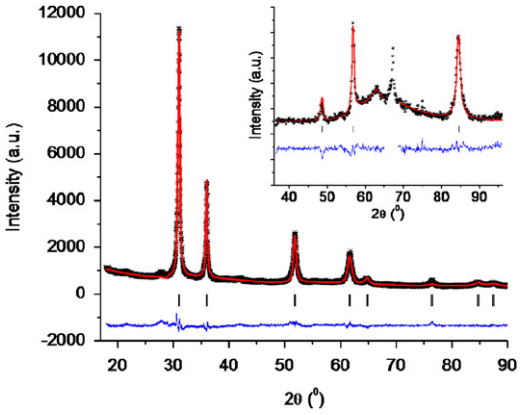

Fig. 6. Rietveld plots of $InVO_{3.54}$ room temperature refinement. Powder X-ray diffraction data Cu$K\alpha_{1,2}$ radiation ($\chi^2 = 2.66$) and the inset shows the powder neutron diffractogram $\lambda = 2.37$ Å ($\chi^2 = 7.17$). The broad background centered at 63° is possibly due to oxygen defect clustering, no such feature is found in the X-ray data. The excluded peak is the vanadium (1 1 0) reflection from the sample container.

oxidation was carried out in oxygen flow. The sample mass gain in Fig. 5 shows two strongly overlapping oxidation steps, where the initial mass gain is significantly larger than the expected value. The major peaks for the DTA trace indicate two oxidation steps. These results are in agreement with the formation of $InVO_4$ impurities during the first oxidation step. In contrast $ScVO_3$ oxidizes in two distinct steps under the same experimental conditions.

3.3. $InVO_{3.5+x}$ and $ScVO_{3.5+x}$ structures

Bulk samples of $ScVO_{3.70}$ and $InVO_{3.54}$ were investigated by powder X-ray and neutron diffraction. The oxygen compositions were determined by TGA. $ScVO_{3.5+x}$ and $InVO_{3.5+x}$ crystallize in space group $Fm\text{-}3m$ with Sc^{3+}/V^{4+} and In^{3+}/V^{4+} disorder on the 4*a* site (0,0,0), respectively. Oxygen is located on the 8*c* site ($\frac{1}{4}, \frac{1}{4}, \frac{1}{4}$) with defect concentrations ranging from 7.5% to 12.5% for $AVO_{3.7}$ and $AVO_{3.5}$, respectively. This is significantly below the percolation limit. Powder X-ray and powder neutron diffraction data collected at room temperature were analyzed by the Rietveld method, plots of both $InVO_{3.54}$ diffractograms and all three $ScVO_{3.70}$ diffractograms are shown in Figs. 6 and 7, respectively. For $InVO_{3.54}$ a total of 14 parameters and for $ScVO_{3.70}$ a total of 17 parameters were refined including scale factors, neutron wavelengths, zero points, peak shape parameters, the unit cell parameter and the Debye–Weller factors. The backgrounds were fitted during the initial cycles of the refinement using a cubic spline and were fixed for the consecutive cycles. The oxygen temperature factors of 10.7(5) and 16(2) Å^2 for $ScVO_{3.70}$ and $InVO_{3.54}$, respectively, are particularly large due to the large defect concentration in this structure. The refinement results are listed in Table 2.

The broad diffraction peaks resulting from the low temperature synthesis are due to small crystalline domains ($D \approx 225(50)$ Å), whose sizes have been determined with the

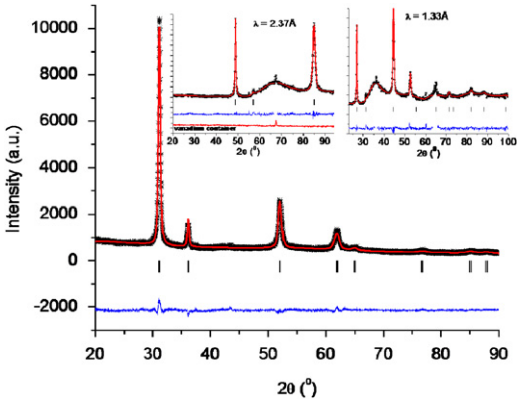

Fig. 7. $ScVO_{3.70}$ room temperature Rietveld plots of a combined powder X-ray and neutron refinement. X-ray Cu$K\alpha_{1,2}$ radiation ($\chi^2 = 1.86$), neutron pattern with $\lambda = 2.37$ Å ($\chi^2 = 3.39$), and $\lambda = 1.33$ Å ($\chi^2 = 6.40$). The excluded regions in the neutron diffractograms are the vanadium (110) and (211) peaks from the sample container. The neutron patterns show broad features at $d = 2.13$ Å corresponding to domain sizes of 20 Å. The pattern underneath the $\lambda = 2.37$ Å diffractogram belongs to the empty vanadium container.

Scherrer Eq. (6)

$$D = 0.9\lambda/B\cos(\theta), \tag{6}$$

where D is the domain size, λ the wavelength, B the integral breadth and θ is the diffraction angle. $InVO_{3.54}$ and $ScVO_{3.70}$ both show a broad peak only visible in the neutron diffractograms at $d = 2.13$ Å with estimated domain sizes of approximately 20 Å. We speculate that these features are a result of oxide defect clusters.

3.4. Oxidation pathway from AVO_3 via $AVO_{3.5+x}$ to AVO_4

The topotactic oxidation of AVO_3 bixbyites to $AVO_{3.5+x}$ defect fluorites is a result of the structural similarities of the bixbyite and the fluorite structures [17]. In the fluorite structure (AO_2) the cations form a c.c.p. structure with the

Table 2
Room temperature crystallographic details for $InVO_{3.54}$ and $ScVO_{3.70}$ as obtained from Rietveld refinements

		$ScVO_{3.70}$			$InVO_{3.54}$		
Space group		*Fm*-3 *m* (227)			*Fm*-3 *m* (227)		
a (Å)		4.9697(3)			4.9863(5)		
V(Å^3)		122.74(1)			123.99(2)		
Z		2			2		
	site	Frac. occ.		Biso(Å^2)	Frac. Occ.		Biso(Å^2)
A^{3+}	4*a*	$\frac{1}{2}$		3.3(2)	$\frac{1}{2}$		2.9(2)
V^{4+}	4*a*	$\frac{1}{2}$		3.3(2)	$\frac{1}{2}$		2.9(2)
O	8*c*	0.925		10.7(5)	0.885		16(2)
		R_p	R_{wp}	χ^2	R_p	R_{wp}	χ^2
XRD[a]		4.13	5.43	1.92	4.57	5.97	2.51
			4781 Data points			4781 Data points	
NPD-1[b]		1.87	2.41	3.17	2.46	3.42	7.17
			795 Data points			795 Data points	
NPD-2[c]		1.79	2.41	6.16			
			795 Data points				
Parameters			17			14	

[a]XRD = X-ray diffraction pattern with $\lambda = 1.540598$, 1.544426 Å.
[b]NPD-1 = neutron diffraction pattern $\lambda(InVO_{3.54}) = 2.3700(9)$Å, $\lambda(ScVO_{3.70}) = 2.3718(5)$Å.
[c]NPD-2 = neutron diffraction pattern with $\lambda = 1.3321(3)$Å.

anions occupying all tetrahedral interstitial sites, removing one out of eight anions in an ordered fashion results in the pyrochlore structure ($A_2B_2O_7$), removing a second anion (across the cubic body diagonal of the first removed anion) results in the bixbyite structure (A_2O_3). Fig. 8 schematically illustrates the anion vacancy relation of the bixbyite and pyrochlore structures to the fluorite structure. We propose that the topotactic oxidation of the bixbyite structure proceeds via statistical addition of one oxygen atom to the vacant anion sites resulting in the defect fluorite structure with space group *Fm*-3 *m*. Further oxidation results in A^{3+}, V^{5+} cation ordering where the small pentavalent vanadium is tetrahedrally coordinated in the zircon structure. We have oxidized the perovskite $LuVO_3$ in oxygen during in-situ powder X-ray diffraction experiments and no $AVO_{3.5}$ intermediate was observed during this reaction. In contrast to the bixbyite phases analogous perovskites AVO_3 oxidize to AVO_4 zircon structures without the formation of an $AVO_{3.5}$ intermediate. Furthermore reductions of the zircon type AVO_4 phases proceed directly to either the AVO_3 bixbyites (A = Sc, In) or perovskites for A = La–Lu. These findings strongly support the topotactic pathway of bixbyite oxidation. The narrow temperature range ($T = 350 \pm 10\,^{\circ}C$) for the synthesis of $InVO_{3.5}$ in carbon dioxide with respect to the broad temperature range for $ScVO_{3.5}$ ($T = 350 \pm 50\,^{\circ}C$) preparation indicates the fragility of $InVO_3$ and $InVO_{3.5}$ with respect to $InVO_4$ in the presence of an oxidant.

3.5. Low temperature magnetic properties of $InVO_{3.5}$ and $ScVO_{3.5}$

D.c. magnetic susceptibility data reveal the presence of V^{4+} in the $AVO_{3.5}$ defect fluorite structures. The high

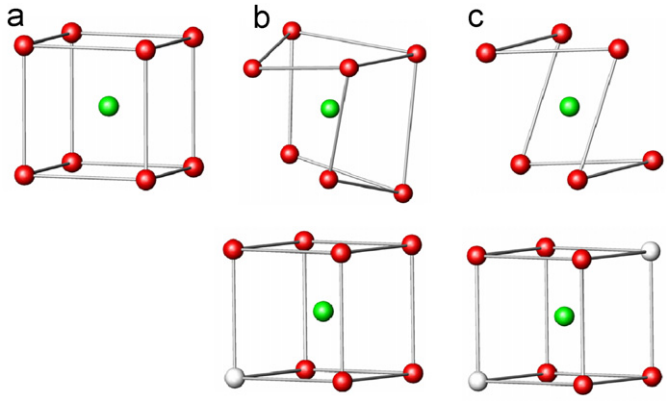

Fig. 8. Schematic illustration of the fluorite structure, green = cation, red = anion. (a) cubic fluorite structure, (b) pyrochlore structure fragment with one oxide vacancy for 8 oxide ions (vacancy ordering is observed), for $AVO_{3.5}$ the vacancies are statistically distributed, (c) bixbyite structure section with two oxide vacancies out of 8 oxide anions. The upper panel shows fragments of actual structures, the lower panel relates the idealized fluorite structure analogues. The connecting lines are shown to guide the eye.

temperature data were fitted with the Curie–Weiss law modified with a temperature independent term, Eq. (7)

$$\chi = \frac{C}{(T-\theta)} + \alpha, \tag{7}$$

where C is the Curie constant, T the temperature, θ the Weiss temperature and α is the temperature independent term. All data were corrected for diamagnetism and sample compositions. The magnetic data for $InVO_{3.54}$ are shown in Fig. 9. The zero-field cooled (ZFC) and field cooled (FC) d.c. susceptibility data superimpose with no signs of hysteresis or any phase transitions. The Curie–Weiss fit for $InVO_{3.54}$ revealed a Curie constant

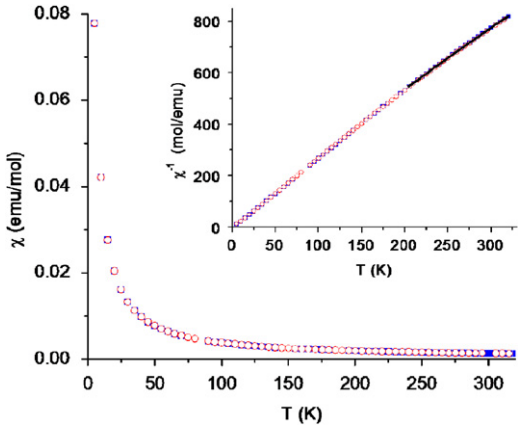

Fig. 9. Low temperature d.c. magnetic susceptibility data for $InVO_{3.54}$ measured in a magnetic field of $H = 0.1$ T.

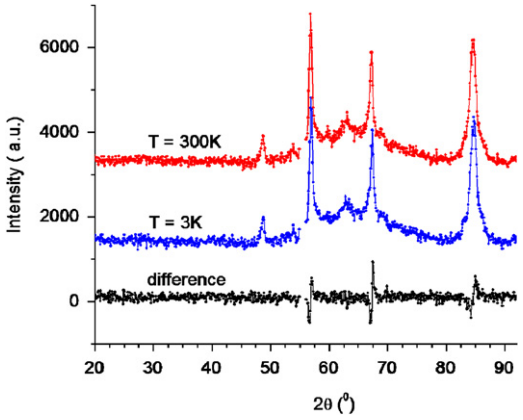

Fig. 10. Powder neutron diffraction patterns ($\lambda = 2.37$ Å) of $InVO_{3.54}$ at $T = 300$ K (red) and 3 K (blue). The difference (3–300 K) is shown at the bottom (black). No magnetic diffraction peaks are observed at 3 K. The only features in the difference plot correspond to the unit cell contraction upon cooling.

$C = 0.355(1)$ emu K mol^{-1}. The expected Curie constant for spin-only V^{4+} is 0.374, whereas a 1:1 ratio of V^{3+}:V^{5+} would result in a Curie constant $C = 0.5$ emu K mol^{-1}. The Curie–Weiss fit clearly indicates the presence of V^{4+} in $InVO_{3.5+x}$. The effective magnetic moment of $\mu_{eff} = 1.75(1)\,\mu_B$ for V^{4+} in $InVO_{3.54}$ is consistent with the expected spin-only magnetic moment for V^{4+} of $1.73\,\mu_B$ and a Weiss temperature of $-2.9(8)$ K. The near zero Weiss-constant indicates negligible spin–spin interactions or canceling antiferromagnetic and ferromagnetic interactions. Low temperature powder neutron diffraction experiments are consistent with the cubic defect fluorite structure in space group *Fm*-3*m*. No magnetic neutron diffraction peaks are observed upon cooling to 3 K. Fig. 10 compares the room temperature and low temperature powder neutron diffraction patterns for $InVO_{3.54}$. The only features observed in the difference plot are due to unit cell contraction upon cooling. The magnetic data rule out a cooperative magnetic ground state and support a paramagnetic state even at the lowest temperatures. Similarly, $ScVO_{3.70}$ low temperature powder neutron diffraction data did not show any evidence of magnetic ordering.

4. Conclusions

We have reported the first synthesis and structure determination of the metastable defect fluorite structure $InVO_{3.5+x}$. The fluorite structure can exist with a range of anion vacancies leading to diverse oxygen stochiometries as shown for $ScVO_{3.5+x}$ and $InVO_{3.5+x}$ ($0.00 \leqslant x \leqslant 0.22$). The oxidation of the bixbyite phases AVO_3 has been followed by in-situ X-ray diffraction and thermal gravimetric analysis. The gradual oxygen uptake in the bixbyite phase is followed by the formation of a defect fluorite structure with variable oxygen content and the final oxidation to AVO_4 containing only pentavalent vanadium. $ScVO_{3.5+x}$ can be readily synthesized in air between 300 and 400 °C, while in contrast pure $InVO_{3.5+x}$ is only accessible close to 350 °C using CO_2 as a gentle oxidant. The preparation of $InVO_{3.5+x}$ is complicated by the low stabilities of the metastable bixbyite and defect fluorite structures, consequently overoxidation to $InVO_4$ is observed even at low temperatures. $InVO_{3.5+x}$ and $ScVO_{3.5+x}$ crystallize in *Fm*-3*m* with A^{3+}/V^{4+} disorder on the 4*a* site and statistical oxygen vacancies on the 8*c* site. $AVO_{3.5}$ phases cannot be obtained via reduction of AVO_4. The oxidative route towards $AVO_{3.5}$ from the parent bixbyite structures confirms the topotactic nature of the reaction. The large temperature factors for the oxygen positions in the $AVO_{3.5+x}$ structures indicate the potential for oxide ion conduction in those phases. The magnetic moments on vanadium in $AVO_{3.5+x}$ do not undergo magnetic ordering at temperatures as low as 3 K. Magnetic susceptibility data confirm the presence of V^{4+} rather then V^{3+} and V^{5+} in $AVO_{3.5}$.

Acknowledgments

The authors are grateful to Craig Bridges (McMaster University) for the magnetic measurements. M.B. gratefully acknowledges funding from NSERC and CFI. L.M.D.C. wishes to thank NRC technicians Raymond Sammon and Travis Dodd for assistance in setting-up the Janis closed cycle refrigerator system on C2.

References

[1] H.C. Nguyn, J.B. Goodenough, Phys. Rev. B 52 (1995) 324–334.
[2] T. Mizokawa, D.I. Khomskii, G.A. Sawatzky, Phys. Rev. B. 60 (1999) 7309.
[3] Y. Ren, T.T.M. Palstra, D.I. Khomskii, E. Pellegrin, A.A. Nugroho, A.A. Menovsky, G.A. Sawatzky, Nature 396 (1998) 441–444.
[4] Miyasaka, Y. Okimoto, M. Iwama, Y. Tokura, Phys. Rev. B. 68 (2003) 100406.
[5] J.-Q. Yan, J.-S. Zhou, J.B. Goodenough, Phys. Rev. B. 72 (2005) 094412.

[6] R.J. Lundgren, L.M.D. Cranswick, M. Bieringer, J. Solid State Chem. 179 (2006) 3599.
[7] A.F. Reid, M.J. Sienko, Inorg. Chem. 6 (1967) 521.
[8] J.A. Alonso, M.T. Casais, M.J. Martinez-Lope, Dalton Trans. 9 (2004) 1294.
[9] R.J. Lundgren, L.M.D. Cranswick, M. Bieringer, Chem. Mater. 19 (2007) 3945.
[10] B.C. Chakoumakos, M.M. Abraham, L.A. Boatner, J. Solid State Chem. 109 (1994) 197.
[11] M. Touboul, P. Toledano, Acta. Crystallogr. B. 36 (1980) 240–245.
[12] M. Touboul, K. Melghit, P. Benard, D. Louer, J. Solid State Chem. 118 (1995) 93–98.
[13] J. Senegas, J.P. Manaud, J. Galy, Acta Crystallogr. B. 31 (1975) 1614–1618.
[14] P. Lacorre, F. Goutenoire, O. Bohnke, R. Retoux, Y. Laligant, Nature 404 (2000) 856.
[15] J.B. Goodenough, Nature 404 (2000) 821.
[16] J. Rodriguez- Carvajal, Full Prof 2k Vers. 3.20, (2005).
[17] A. Ambrosini, A. Duarte, K.R. Poepplemeier, M. Lane, C.R. Kannewurf, T.O. Mason, J. Solid State Chem. 153 (2000) 41–47.